**The Compact Muon Solenoid Experiment**

# Conference Report

Mailing address: CMS CERN, CH-1211 GENEVA 23, Switzerland

# Operation and Performance of the CMS Outer Tracker

Erik Butz on behalf of the CMS Collaboration

**Abstract**

The CMS Silicon Strip Tracker with its more than 15000 silicon modules and $200\,\mathrm{m}^2$ of active silicon area has been running together with the other subsystems of CMS for several years. We present the performance of the detector in the LHC Run 2 data taking. Results for signal-to-noise, hit efficiency and single hit resolution will be presented. We review the behavior of the system when running at beyond-design instantaneous luminosity and describe challenges observed under these conditions. The evolution of detector parameters under the influence of radiation damage will be presented and compared to simulations.

Presented at *VERTEX2017, 26th International Workshop on Vertex Detectors*

# Operation and Performance of the CMS Outer Tracker

**Erik Butz on behalf of the CMS Collaboration**[*]

*Karlsruhe Institute of Technology*

*E-mail:* erik.butz@cern.ch

The CMS Silicon Strip Tracker with its more than 15000 silicon modules and $200\,m^2$ of active silicon area has been running together with the other subsystems of CMS for several years. We present the performance of the detector in the LHC Run 2 data taking. Results for signal-to-noise, hit efficiency and single hit resolution will be presented. We review the behavior of the system when running at beyond-design instantaneous luminosity and describe challenges observed under these conditions. The evolution of detector parameters under the influence of radiation damage will be presented and compared to simulations.

*The 26th International Workshop on Vertex Detectors*
*10-15 September, 2017*
*Las Caldas, Asturias, Spain*

---

[*]Speaker.

# 1. Introduction

The CMS Silicon Strip Tracker (SST) [1][2] was installed in the CMS experiment [3] at the end of 2007. The detector has been connected, checked out and commissioned and has been running together with CMS for the last nine years, first in extended cosmics campaigns and later in physics data taking during the LHC Run 1 and Run 2.

The system is still the largest of its kind with 15148 individual detector modules and an active area of $200\,\mathrm{m}^2$ of silicon. The layout of the SST is shown in Fig. 1. The SST is organized into
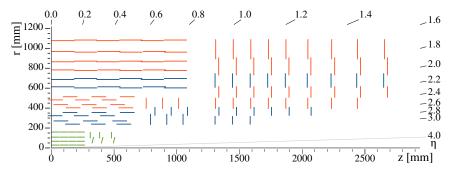


**Figure 1:** An *rz* view of one quarter of the CMS silicon strip tracker. Layers with so-called *stereo modules* (see text for details) are drawn as blue lines. Modules in the TIB, TID and first four rings of the TEC have $320\,\mu\mathrm{m}$ thick silicon sensors, $500\,\mu\mathrm{m}$ silicon is used in the TOB and rings 5-7 of the TEC.

different sub-structures. The central part has a barrel type arrangement with concentric layers of silicon modules with their surface parallel to the beam axis. The *Tracker Inner Barrel* (TIB) contains four layers of silicon modules between $25.5\,\mathrm{cm}$ and $49.8\,\mathrm{cm}$ of radius. At higher radii, the *Tracker Outer Barrel* (TOB) contains six layers ranging from $60.8\,\mathrm{cm}$ to $108.0\,\mathrm{cm}$. In the forward direction the SST contains two sub-detectors with disk like structure where the modules are oriented perpendicular to the beam. The *Tracker Inner Disks* (TID) complement the TIB coverage in the forward region with three disks at *z* positions between $70\,\mathrm{cm}$ and $105\,\mathrm{cm}$ from the interaction point. The TID disks contain three concentric rings of silicon modules. The SST is completed by the two large *Tracker Endcaps* (TEC) which consist of 9 disks of silicon modules. The number of rings decreases from seven for the first three disks to only the outer four rings for the last disk. The TIB, TID and inner four rings of the TECs have silicon modules with a single silicon wafer with $320\,\mu\mathrm{m}$ thickness. The strip pitch varies from $80\,\mu\mathrm{m}$ to $141\,\mu\mathrm{m}$. The TOB and rings 5-7 in the TEC contain modules with two silicon wafer daisy chained. This larger cell size can be afforded because of the reduced occupancy further away from the interaction point. The increased strip length leads to higher capacitive noise. To offset this and maintain a sufficiently high signal to noise ratio, silicon with $500\,\mu\mathrm{m}$ thickness is used. The strip pitch in the outer regions varies from $122\,\mu\mathrm{m}$ to $205\,\mu\mathrm{m}$. The first two layers of TIB and TOB and the rings 1 and 2 (1,2 and 5) of the TID (TEC) contain double-sided or stereo modules where two detector modules are glued back-to-back and in one of them the strips are rotated by $100\,\mathrm{mrad}$ so that together they provide an effective 3D space point reconstruction.

The individual silicon strips are read out by the APV25 ASIC[4]. The APV25 reads out 128 strips and has an analog pipeline with 192 cells for each strip which allows for the buffering of the strip signal while waiting for a level 1 accept signal (L1A) from the CMS global trigger. Upon

receipt of an L1A, the APV25 chips read out, amplify and shape the signal from the corresponding pipeline cells. The APV25 shaper output has a rise time of 50 ns and a falling time of several hundred ns. In order to minimize the contribution from adjacent events when the LHC runs with proton bunches spaced by 25 ns, the APV25 can perform a three-sample weighted average of three pipeline cells which are read out for a given L1A to perform an effective deconvolution of the signal. With this procedure, the signal is effectively contained within one LHC bunch crossing. The signal from two APV25 chips is time multiplexed by the APVMUX ASIC and converted from an electric to an optical signal on the *Analog Opto-Hybrid* (AOH). The AOH contains a linear laser driver (LLD) with four switchable gain stages which allow for the equalization of the optical signal strength across different detector parts. The optical signal is generated using edge-emitting InGaAsP devices and is transmitted over 60-100 m to the *Underground Service Cavern* (USC) outside of the radiation zone. It is received by the *Front End Drivers* (FED). The FED is a 9U VME board with eight identical inputs to receive a total of up to 96 individual readout fibers from the detector to read out a maximum of 192 APV25 chips per FED. In normal physics data taking, the signal from the APV chips is un-multiplexed, the pedestal value of each strip is subtracted, common mode is removed per chip and per event and cluster finding is performed. A threshold of five(two) times the noise of strip is applied for single(multi) strip clusters and only information from strips passing these cuts is shipped out to the CMS central data acquisition.

The programming of the detector modules is performed by *Front End Controller* (FEC) boards which communicate via bi-directional optical links with control token ring networks inside the detector. The token rings consist of several *Clock and Control Units* (CCU), which transmit configuration parameters to the modules using the $I^2C$ protocol, as well as clock, trigger and fast reset signals on a dedicated communication line. A total of 356 control rings are used in the tracker.

Power to the SST is supplied by 964 CAEN 4601 power supply modules (PSM) which contain two power supply units (PSU) each. The PSUs supply 1.25 V and 2.5 V of low voltage and up to 600 V of sensor bias voltage to the detector modules. More details about powering can be found in [5].

The SST is cooled by two non-redundant cooling plants which circulate mono-phase $C_6F_{14}$ to the detector via two times 90 cooling loops. Due to an over-pressure incident in 2009, five cooling loops developed leaks in non-accessible locations and had to be closed. The detector parts affected by this are passively cooled via the mechanical structure and continue to operate with the rest of the SST.

## 2. Commissioning of the Strip Tracker

During the LHC long shutdown one (LS1), the operating temperature of the SST was lowered to a coolant temperature of -15°C. The system was re-calibrated to adjust operational parameters of the readout electronics to the new operating conditions. Some components are particularly susceptible to temperature changes, e.g. the gain of the optical links is expected to change by 0.8%/K [6]. During year end technical stops of the LHC and shorter technical stops during the the running year, the calibration of most part of the readout chain is repeated to ensure that channels are at their optimal working point. The full commissioning procedure of the tracker is described in [7], the steps which need to be repeated regularly are recapped below.

The first step in the re-calibration is the optical link setup run (also called *gain* or *opto scan*). It is a nested loop in which the four gain stages are scanned and for each of the steps, the laser bias is swept through the full available range of 0–22.5 mA. The choice of bias point is made to ensure that the laser diode will send a non-zero signal for the minimal expected signal and that the FED receivers are not saturated for the highest expected signal. The gain setting is chosen to arrive closest to a link gain of 0.86 V/V, where the input is a $\pm400$ mV differential signal from the APV25 (a "digital 1" also called *tick mark*), issued by the APV25 every 70 clock cycles in absence of a L1 trigger signal. The FED receiver as last step in the chain has a conversion factor of about 1 ADC count/mV.

In Fig. 2, the results from a recent gain scan are shown. The relative selection frequency of the four gain stages is essentially unchanged since LS1 suggesting no appreciable loss of laser driver efficiency. The acquired radiation dose after LS1 corresponds to about 75 fb$^{-1}$. Fig. 2, right shows the resulting distribution of the height of the tick mark after the optimization procedure. The vast majority of the optical links are centered around the target gain of 0.86 V/V which corresponds to about 690 ADC counts. Some links with tick mark heights of below 500 ADC counts can be seen. These correspond to detector components which are temporarily or permanently faulty and are excluded from the data acquisition.
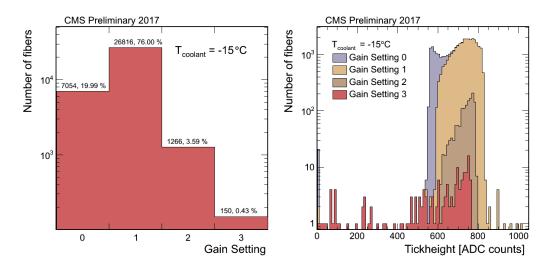


**Figure 2:** Left: Chosen gain setting at -15°C coolant temperature in August 2017. Right: Distribution of tickheights per laser driver gain setting for data taken in August 2017 at -15°C coolant temperature.

After the optical link tuning, the pedestal and noise values of the individual silicon strips have to be measured. This is done by recording non-zero suppressed data in periods with no beam using a low frequency cyclic trigger. The pedestal value of a channel is the mean value of the signal of the strip over few thousand events when no particle signal is present. The noise is calculated as the variance of this distribution. The total noise of the detector comes from several sources: the silicon sensor, the APV25 chip, APVMUX, and AOH components as well as the FED receiver. The noise from the silicon sensor has a capacitive component that is expected to scale linearly with the length of the strips. In Fig. 3 the scaling behavior as function of strip length is shown and compared to results from post-installation data taking. It can be seen that there is a clear linear scaling with strip

length as expected. The data are fitted with a first order polynomial. The extracted coefficients for data from 2017 are compatible with the results obtained shorter after installation.
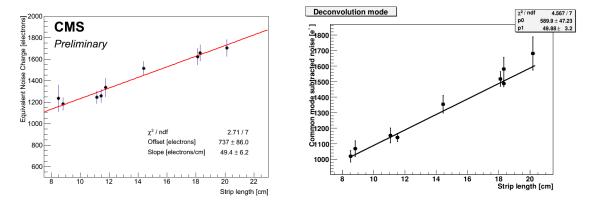


**Figure 3:** Noise performance as function of strip length. Right figure from [3].

After all commissioning steps, the fraction of active readout channels in the SST is around 96.5%.

## 3. Performance of the Strip Tracker during LHC Run 2

The SST is going into its sixth year of high energy data taking with LHC beams, and the performance of the system is monitored continuously.

The signal to noise ratio (S/N) for hits on reconstructed particle trajectories is a commonly used figure of merit for the performance of the system during collision data taking. The measured particle signal is corrected for the effective length of the trajectory inside the silicon sensor. Two example distributions are shown in Fig. 4 for the TIB and TOB. The distribution can be fitted with
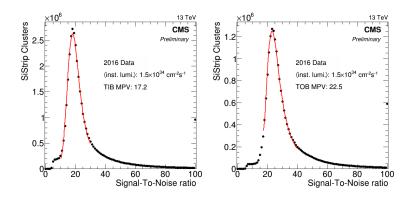


**Figure 4:** Signal to noise for clusters on reconstructed particle tracks for the TIB (left) and TOB (right). The particle signal is corrected for the length of the trajectory inside the silicon sensor.

the convolution of a Landau and a normal distribution. The most probable value (MPV) of this distribution is a measure of the S/N for a given detector part. A summary of the MPVs for the individual parts of the SST during 2016 and 2017 is given in Tab. 1.

**Table 1:** Most probable value of a convoluted Landau and normal distribution fit to the signal to noise ratio distributions for different parts of the SST. The particle signal is corrected for the length of the trajectory inside the silicon volume. For the TEC subdetectors, sensors with 320 μm (thin) and 500 μm (thick) of silicon are listed separately.

| Sensor type | S/N [MPV] (2016) | S/N [MPV] (2017) |
|---|---|---|
| TIB | 17.2 | 17.0 |
| TID | 16.7 | 16.7 |
| TOB | 22.5 | 22.4 |
| TEC (thin) | 18.0 | 17.9 |
| TEC (thick) | 22.5 | 22.4 |

In late 2015 and early 2016, the SST observed a decrease in signal to noise associated also with loss of hits on tracks. This behavior was traced to saturation effects in the pre-amplifier of the APV25 readout chip. The drain speed of the pre-amplifier was affected more strongly by the change in operating temperature than anticipated, leading to too slow discharge of the amplifier under high occupancy conditions. The drain speed was changed to allow for faster recovery. This measure completely removed the effect on the signal to noise ratio and hit efficiency. The effect on the signal to noise is illustrated in Fig. 5 where it is shown for clusters on tracks in the TOB layer 1, which was the detector region worst affected by the effect. It can be seen that the shape of the distribution deviates from the normal shape with a downward shifted MPV and an increased population in the tail end of the distribution. The corresponding effect on the single hit reconstruction efficiency is shown in Fig. 6. It can be seen that in runs affected by the pre-amplifier saturation, the efficiency drops quickly as function of the instantaneous luminosity and a loss of several percent is visible around $1 \times 10^{34} \mathrm{cm}^{-2}\mathrm{s}^{-1}$. After the change of pre-amplifier drain speed, the inefficiency is greatly reduced and an efficiency close to 100% is observed even at beyond design instantaneous luminosity.
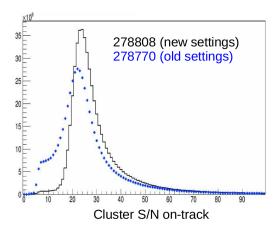


**Figure 5:** Signal to noise for clusters on reconstructed particle tracks in TOB layer 1 for two different runs in summer 2016. The first run (278770, blue dots) is affected by saturation effects in the APV25 pre-amplifier which results in downward shift of the most probable value and an increased population in the low-end tail of the distribution. In the second run (278808, black line) after the change of pre-amplifier drain speed, the signal to noise distribution has recovered to the standard shape [9].
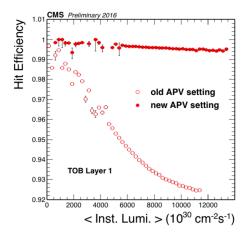
5

**Figure 6:** Hit efficiency as function of the the instantaneous luminosity for the modules in TOB layer 1 for runs before the change of pre-amplifier drain speed (open circles) and after (filled circles).

The spatial resolution of reconstructed clusters in the tracker is estimated using the so-called *pair method*. For this, hits within one layer of the SST are considered where two detector modules have a sufficient overlap to be crossed by the same particle trajectory. The effects of multiple scattering, which otherwise would have significant influence on the results, can be minimized with this approach. Only tracks with a transverse momentum larger than 3 GeV/$c$, more than six hits in layers of the SST and the pixel detector and good $\chi^2$ probability of the track fit are considered. The clusters under study in the two silicon modules need to be of the same size. The spatial resolution for clusters in a single sensor is estimated from

$$\sigma_{hit} = \sqrt{\frac{\sigma_{pred-meas}^2 - \sigma_{meas}^2}{2}} \tag{3.1}$$

where $\sigma_{pred-meas}$ is the double difference of measured and predicted position between the two sensors and $\sigma_{meas}$ is the difference between the two measured positions; as these numbers combine the resolution effects from both sensors, the result is divided by $\sqrt{2}$ to obtain the resolution for a single sensor. The results for the position resolution are summarized in Fig. 7. It can be seen that the resolution improves for smaller strip pitches as can be expected. TOB sensors with similar strip pitches to TIB sensors have slightly better resolution which can be attributed to the higher signal to noise ratio. Cluster sizes above one show improved resolution as can be expected from charge sharing and the use of the analog readout of the tracker.

## 4. Radiation Effects

Radiation effects are expected in many parts of the SST and will alter the behavior of the system over time. Two main aspects will be the focus in the following: leakage current evolution in the silicon sensors and radiation effects in the optical link system.

The evolution of the parameters of the AOHs under irradiation has been investigated prior to the installation in the tracker [8]. Two main effects are expected: increase in laser threshold current, i.e. the minimum needed current to obtain a non-zero signal from the laser diode, and
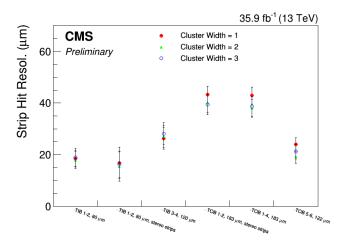
**Figure 7:** Single hit resolution in the SST for different sensor geometries obtained with the pair method (see main text for details).

loss of laser efficiency, i.e. a reduction of the optical output signal for a given input signal. As has been discussed in Sec. 2, no appreciable loss in efficiency is observed at the time of writing of this report. The evolution of laser threshold current is investigated as function of time using the results from optical link setup runs. This is shown in Fig. 8 where the relative increase in threshold current is shown for lasers in the TIB. The results are separated for different layers. It can be seen that the threshold current increases in periods of high luminosity running and anneals during periods with low intensity running (e.g. heavy-ion collisions) and periods without beam. As can be expected, the observed increase in threshold current is largest in the first layer of the TIB and gradually decreases for higher radii. The observed increase in threshold current is compatible or lower than what is expected from [8], suggesting that there is sufficient margin to operate the optical link system of the SST until its end of life.
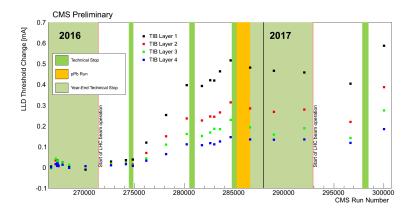


**Figure 8:** AOH laser threshold current increase for modules in the TIB. The results are shown for the different layers of the TIB separately. Year-end technical stop and short technical stops are indicated as colored boxes, as are low intensity running periods with heavy ion collisions.

The evolution of the silicon sensor leakage current is the second topic presented here. The modeling of the sensor leakage current is done based on the Hamburg Model [10] with param-

eters adapted to the sensors used in the SST. The temperature evolution is taken into account in the simulation by using measurements from the detector itself. At certain "anchor points", measurements are obtained via the *Detector Control Units* (DCU) which are custom ASICs installed on each detector module of the SST. The DCUs allow for the readout of the temperature of the silicon sensor and its leakage current (for modules with two sensors, only a single measurement is available). The projection of the leakage current uses the initial values of leakage current and temperature. The temperature evolution is modeled using relative measurements from few, representative measurements inside the SST. The radiation environment modeling is obtained from FLUKA simulations [11]. In Fig. 9 the evolution of the leakage current of one module in the TIB layer 1 is compared to the simulation. Good agreement can be seen between the two curves. The measured values are obtained from the DCU; the readings are only available when the detector is powered and the data acquisition is running. For certain representative moments the simulation is compared to the measured value for the full SST. This comparison can be seen in Fig. 10 where for a date in late 2016 the leakage current as measured by the DCUs is compared to the equivalent predicted value. In general good agreement can be seen, the predictions are compatible with the observed values within the uncertainties on the fluence simulation and the modeling parameters.
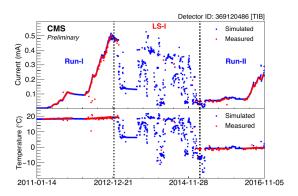


**Figure 9:** Leakage current evolution for one module in the TIB layer 1 as function of time. Blue points show the predicted evolution of the leakage current, red points show measurements obtained using the DCU.
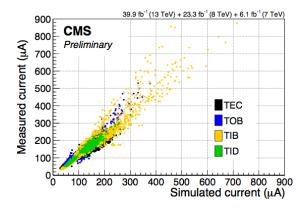


**Figure 10:** Leakage current measured by DCU compared to prediction in late 2016.

## 5. Summary and Outlook

The CMS Silicon Strip Tracker continues to efficiently take data together with the other subsystems of the CMS experiment and delivers high quality tracking to CMS physics analyses. The system has been re-calibrated at lower operating temperatures after the LHC long shutdown one, and continuous efforts are undertaken to keep the system performance as good as possible. The signal to noise performance is excellent and in agreement with expectations. The problem of saturation effects in the APV25 pre-amplifier which resulted in degraded performance of the system under high occupancy conditions during late 2015 and early 2016 could be successfully resolved. The single hit efficiency is very high and stable, good spatial resolution is observed in agreement with expectations and benefiting from the analog readout of the system.

Radiation effects are becoming visible in many parts of the system. The performance of the optical link system is closely monitored, and the observed radiation effects suggest ample margin up to the expected end of life of the system. The leakage current evolution in the different parts of the SST is being monitored and compared to simulations. Good agreement is found between the two suggesting a good understanding of the evolution of the system to model its behavior in future.

## References

[1] CMS Collaboration, "CMS, Tracker Technical Design Report," CERN-LHCC-98-06, CMS-TDR-5.

[2] CMS Collaboration, "Addendum to the CMS Tracker TDR by the CMS Collaboration," CERN-LHCC-2000-016, CMS-TDR-5-add-1.

[3] CMS Collaboration, "The CMS Experiment at the CERN LHC," JINST **3**, S08004 (2008). doi:10.1088/1748-0221/3/08/S08004

[4] M. J. French *et al.*, "Design and results from the APV25, a deep sub-micron CMOS front-end chip for the CMS tracker," Nucl. Instrum. Meth. A **466**, 359 (2001)

[5] S. Paoletti *et al.*, "The powering scheme of the CMS silicon strip tracker", in 10th Workshop on Electronics for LHC and future experiments, CERN-2004-010, CERN-LHCC-2004-030, http://cdsweb.cern.ch/record/814088

[6] S. Dris, K. Gill, J. Troska and F. Vasey, "Predicting the Gain Spread of the CMS Tracker Analog Readout Optical Links" , CMS-NOTE-2006-145, http://cdsweb.cern.ch/record/1000407

[7] R. Stringer [CMS Collaboration], "Commissioning the CMS Silicon Strip Tracker prior to Operations with Cosmic Ray Muons" , CMS-NOTE-2009-021, http://cdsweb.cern.ch/record/1291201

[8] R. Macias, M. Axer, S. Dris, K. Gill, R. Grabit, E. Noah, J. Troska and F. Vasey, "Advance validation of radiation hardness and reliability of lasers for CMS optical links," IEEE Trans. Nucl. Sci. **52**, 1488 (2005). doi:10.1109/TNS.2005.855812

[9] shown at 127th LHCC Open Session, CMS Status Report, https://indico.cern.ch/event/563488

[10] M. Moll, "Radiation damage in silicon particle detectors: Microscopic defects and macroscopic properties," DESY-THESIS-1999-040.

[11] CMS Collaboration, "FLUKA particle flux maps for CMS Detector", https://cds.cern.ch/record/1612355